Inorganic Chemistry

Article

pubs.acs.org/IC

Single-Molecule Magnetism in Three Related $\{Co^{III}_2Dy^{III}_2\}$-Acetylacetonate Complexes with Multiple Relaxation Mechanisms

Stuart K. Langley, Nicholas F. Chilton, Boujemaa Moubaraki, and Keith S. Murray*

School of Chemistry, Monash University, Building 23, Clayton, Victoria 3800, Australia

Supporting Information

ABSTRACT: Three new heterometallic complexes with formulas of $[Dy^{III}_2Co^{III}_2(OMe)_2(teaH)_2(acac)_4(NO_3)_2]$ (**1**), $[Dy^{III}_2Co^{III}_2(OH)_2(teaH)_2(acac)_4(NO_3)_2]\cdot 4H_2O$ (**2**), and $[Dy^{III}_2Co^{III}_2(OMe)_2(mdea)_2(acac)_4(NO_3)_2]$ (**3**) were characterized by single-crystal X-ray diffraction and by dc and ac magnetic susceptibility measurements. All three complexes have an identical "butterfly"-type metallic core that consists of two Dy^{III} ions occupying the "body" position and two diamagnetic low-spin Co^{III} ions occupying the outer "wing-tips". Each complex displays single-molecule magnet (SMM) behavior in zero applied magnetic field, with thermally activated anisotropy barriers of 27, 28, and 38 K above 7.5 K for **1**−**3**, respectively, as well as observing a temperature-independent mechanism of relaxation below 5 K for **1** and **2** and at 3 K for **3**, indicating fast quantum tunneling of magnetization (QTM). A second, faster thermally activated relaxation mechanism may also be active under a zero applied dc field as derived from the Cole−Cole data. Interestingly, these complexes demonstrate further relaxation modes that are strongly dependent upon the application of a static dc magnetic field. Dilution experiments that were performed on **1**, in the $\{Y^{III}_2Co^{III}_2\}$ diamagnetic analog, show that the slow magnetic relaxation is of a single-ion origin, but it was found that the neighboring ion also plays an important role in the overall relaxation dynamics.

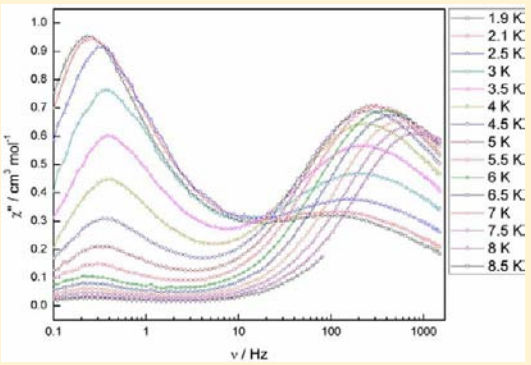

INTRODUCTION

The synthesis of lanthanide-containing coordination complexes that display single-molecule magnet (SMM) behavior is a field that continues to grow at a significant rate.[1] Lanthanide ions display interesting magnetic behavior because of their large magnetic moments and anisotropy. SMM behavior originates from the blocking of a magnetic moment in a particular direction via an anisotropy barrier at sufficiently low temperatures.[2] Under these conditions, the individual molecules display magnetic hysteresis, thus offering potential avenues toward information storage.[3] Other such applications that have been considered for lanthanide-based nanomagnetic materials, SMM-based or otherwise, include their uses as molecular spin qubits that are relevant to quantum computation and as molecular objects for molecular spintronics.[3] Remarkably, it was shown that SMM behavior can arise from a single lanthanide ion, which was originally reported for a terbium bisphthalocyanine complex.[4] This resulted in the revival of lanthanide-based molecular magnetism, with numerous such mono- and, as an extension, polynuclear complexes being reported.[5] Larger anisotropy barriers were subsequently developed in lanthanide-based materials in comparison to those of transition-metal clusters;[6] however, the quantum tunneling of magnetization (QTM) is also generally fast in such systems.[7] This is a problem in the Ln area because the spins tend to tunnel very quickly at zero magnetic field and hence no significant hysteresis is observed. In an attempt to overcome this, Long and co-workers introduced strong magnetic exchange into dinuclear Tb^{III} and Dy^{III} complexes via the interaction of a radical species. This resulted in the suppression of the QTM at zero field with magnetic hysteresis observed at up to 14 K for the Tb^{III} complex, which is the highest thus far reported.[8] Lanthanide complexes also allow for the observation of various unusual magnetic phenomenon such as noncollinear spins resulting in toroidal moments[9] and the presence of multiple relaxation mechanisms of the magnetization within a single molecule.[5i,6d,10] Understanding the role that the various factors play in affecting the relaxation mechanism(s) (thermal and QTM pathways) in lanthanide-based systems, such as exchange interactions and chemical modifications of the molecule, is likely the key to developing more efficient and better performing SMMs. This may be achieved by comparing existing SMM-type complexes in which similar motifs can be studied by making sequential changes to the molecule to see how they will affect the dynamic magnetic behavior. Some efforts at correlating the low-temperature spin dynamics with the distortion of the geometry around the metal ion(s) have recently been reported and show the role played by the local symmetry around the Ln^{III} ions.[11]

Received: March 31, 2013
Published: May 29, 2013

Table 1. Crystallographic Data for Compounds 1−3

	1	2	3
formula[a]	$Co_2Dy_2C_{34}H_{60}O_{22}N_4$	$Co_2Dy_2C_{32}H_{64}O_{26}N_4$	$Co_2Dy_2C_{32}H_{56}O_{20}N_4$
M, g mol^{-1}	1319.72	1363.67	1259.67
crystal system	triclinic	monoclinic	triclinic
space group	$P\bar{1}$	$P2_1/c$	$P\bar{1}$
a (Å)	10.050(2)	14.0879(9)	8.6711(6)
b (Å)	10.990(2)	11.9553(8)	11.9885(8)
c (Å)	11.780(2)	16.5970(11)	12.4358(8)
α (deg)	68.30(3)	90	117.342(2)
β (deg)	69.38(3)	91.237(2)	99.948(2)
γ (deg)	75.21(3)	90	100.614(2)
V (Å^3)	1119.7(4)	2794.7(3)	1078.52(12)
T (K)	100(2)	123(2)	123(2)
Z	1	2	1
ρ_{calc} (g cm^{-3})	1.957	1.611	1.939
λ (Å)[b]	0.71070	0.71073	0.71073
data measured	13 440	19 072	9843
ind. reflns	3607	6389	6346
R_{int}	0.0625	0.0384	0.0249
reflns with $I > 2\sigma(I)$	3565	5172	5291
parameters	295	342	277
restraints	0	37	0
R1[c] (obs), wR2[c] (all)	0.0470, 0.1275	0.0413, 0.1138	0.0524, 0.1129
GOF	1.168	1.062	1.160
largest residuals/e Å^{-3}	2.597, −3.132	1.717, −1.196	4.119, −1.893

[a]Including solvate molecules. [b]Graphite monochromator. [c]R1 $=\Sigma||F_o| - |F_c||/\Sigma|F_o|$, wR2 $= \{\Sigma[w(F_o^2 - F_c^2)^2]/\Sigma[w(F_o^2)^2]\}^{1/2}$.

With this in mind, we have recently reported several heterometallic tetranuclear 3d/4f complexes of the $\{Co^{III}_2Dy^{III}_2\}$-type that utilize amine-based polyalcohol and carboxylate ligands.[12] We studied their dynamic magnetic susceptibility behavior and found large thermal energy barriers to magnetic reversal as well as QTM that was effectively reduced when compared to that of many similar dinuclear lanthanide-based SMMs.[13] We also determined that the slow magnetic relaxation was of a single-ion origin and that the QTM was reduced as a consequence of the interaction with the neighboring Dy^{III} ion within the same molecule. We have followed up on this work by looking at the replacement of various ligands around the above-mentioned $\{Co^{III}_2Dy^{III}_2\}$ clusters to determine how these chemical modifications may affect the single-molecule magnet behavior within this core type. The replacement of the carboxylate ligands for acetylacetonate (acac) has allowed us to isolate several related complexes that all have the same heterometallic butterfly motif as previously reported.[12a] Herein, we present three new complexes with formulas of $[Dy^{III}_2Co^{III}_2(OMe)_2(teaH)_2(acac)_4(NO_3)_2]$ (**1**), $[Dy^{III}_2Co^{III}_2(OH)_2(teaH)_2(acac)_4(NO_3)_2]\cdot 4H_2O$ (**2**), and $[Dy^{III}_2Co^{III}_2(OMe)_2(mdea)_2(acac)_4(NO_3)_2]$ (**3**) ($teaH_3$ = triethanolamine and $mdeaH_2$ = methyldiethanolamine). The complexes that were isolated differ from each other in the alkoxide/hydroxide group that is present and bridges the two Dy^{III} ions as well as in the amine-based polyalcohol ligand that was used. These then differ from the previously reported $\{Co^{III}_2Dy^{III}_2\}$ clusters via the coordination environments that were found around the Co^{III} and Dy^{III} ions. The static and dynamic magnetic properties were studied, with each displaying single-molecule magnet behavior. However, the relaxation dynamics of each complex differed significantly from those that were observed for the previously reported butterfly structures. Furthermore, multiple mechanisms for magnetic relaxation are observed in zero and upon application of a static dc magnetic field.

EXPERIMENTAL SECTION

General Information. All reactions were carried out under aerobic conditions. All chemicals and solvents were obtained from commercial sources and used without further purification. Elemental analysis (CHN) was carried out by Campbell Microanalytical Laboratory, University of Otago, Dunedin, New Zealand. IR spectra were recorded on a Bruker Equinox 55 spectrometer with an ATR sampler provided by Specac, Inc., and the samples were run neat.

*Synthesis of $[Dy^{III}_2Co^{III}_2(OMe)_2(teaH)_2(acac)_4(NO_3)_2]$ (**1**).* $Co(acac)_2\cdot 2H_2O$ (0.15 g, 0.5 mmol) and $Dy(NO_3)_3\cdot 6H_2O$ (0.22 g, 0.5 mmol) were dissolved in MeOH (20 mL), followed by the addition of triethanolamine (0.07 mL, 0.5 mmol) and triethylamine (0.3 mL, 2.0 mmol) to give a purple solution. This was stirred for 2 h after which the solution had turned blue-green. This was subsequently layered with diethylether (Et_2O), and within 2 to 3 days the dark-green crystals of **1** had appeared in an approximate yield of 65%. Anal. Calcd (found) for **1**: $Co_2Dy_2C_{34}H_{60}O_{22}N_4$: C, 30.94 (30.90); H, 4.58 (4.62); N, 4.25 (4.44). Selected IR data, ATR (cm^{-1}): 1600 (s), 1575 (s), 1518 (s), 1457 (m), 1435 (m), 1384 (s), 1261 (w), 1123 (m), 1090 (w), 1068 (w), 1037 (w), 1013 (s).

*Synthesis of $[Dy^{III}_2Co^{III}_2(OH)_2(teaH)_2(acac)_4(NO_3)_2]\cdot 4H_2O$ (**2**).* $Co(acac)_2\cdot 2H_2O$ (0.45 g, 1.5 mmol) and $Dy(NO_3)_3\cdot 6H_2O$ (0.22 g, 0.5 mmol) were dissolved in MeCN (20 mL), followed by the addition of triethanolamine (0.07 mL, 0.5 mmol) to give a brown solution. This was stirred for 2 h after which the solution had turned green. This was subsequently layered with diethylether (Et_2O), and within 2 to 3 days the blue-green crystals of **2** had appeared in an approximate yield of 57%. Anal. Calcd (found) for **2**: $Co_2Dy_2C_{32}H_{64}O_{26}N_4$: C, 28.18 (28.30); H, 4.73 (4.72); N, 4.11 (4.32). Selected IR data, ATR (cm^{-1}): 1565 (s), 1521 (s), 1472 (m), 1457 (m), 1425 (m), 1363 (m), 1286 (s), 1086 (m), 1026 (m).

*Synthesis of $[Dy^{III}_2Co^{III}_2(OMe)_2(mdea)_2(acac)_4(NO_3)_2]$ (**3**).* Complex **3** was prepared the same as **1** except that $mdeaH_2$ (0.06 mL, 0.5 mmol) was used in place of $teaH_3$. A green-brown solution was formed

dx.doi.org/10.1021/ic400789k | Inorg. Chem. 2013, 52, 7183−7192

after the addition of the base. This was then stirred for 2 h to give a blue-green solution that was subsequently layered with diethylether (Et_2O). Within 2 to 3 days, the green crystals of **3** had appeared in an approximate yield of 65%. Anal. Calcd (found) for **3**: $Co_2Dy_2C_{32}H_{56}O_{20}N_4$: C, 30.51 (30.60); H, 4.48 (4.32); N, 4.45 (4.64). Selected IR data, ATR (cm^{-1}): 1600 (s), 1580 (s), 1510 (s), 1436 (m), 1382 (s), 1306 (s), 1262 (m), 1146 (m), 1090 (m), 1013 (s).

X-ray Crystallography. X-ray measurements of **1** were performed at 100(2) K at the Australian Synchrotron MX1 beamline. The data collection and integration were performed with the Blu-Ice[14] and XDS[15] software programs. Compounds **2** and **3** were measured at 123(2) K using a Bruker Smart Apex X8 diffractometer with Mo Kα radiation. Data collection and integration were performed with the SMART and SAINT+ software programs and were corrected for absorption using the Bruker SADABS program. Compounds **1**−**3** were all solved by direct methods (SHELXS-97) and refined (SHELXL-97) by full-matrix least-squares on all F^2 data.[16] The crystallographic data and refinement parameters for **1**−**3** are summarized in Table 1. The crystallographic details are available in the Supporting Information (SI) in CIF format. CCDC nos. 931 477−931 479. These data can be obtained free of charge from the Cambridge Crystallographic Data Centre via www.ccdc.cam.ac.uk/data_request/cif.

Magnetic Measurements. The magnetic susceptibility measurements were carried out with a Quantum Design SQUID magnetometer MPMS-XL 7 operating between 1.8 and 300 K for dc fields ranging from 0 to 5 T. The microcrystalline samples were dispersed in Vaseline to avoid torquing of the crystallites. The sample mulls were contained in a calibrated gelatin capsule held at the center of a drinking straw that was fixed at the end of the sample rod. ac susceptibilities were carried out under an oscillating ac field of 3.5 Oe with frequencies ranging from 0.1 to 1500 Hz.

RESULTS AND DISCUSSION

Structural Descriptions. *Crystal Structures of* $[Dy^{III}_2Co^{III}_2(OMe)_2(teaH)_2(acac)_4(NO_3)_2]$ *(**1**),* $[Dy^{III}_2Co^{III}_2(OH)_2(teaH)_2(acac)_4(NO_3)_2]\cdot 4H_2O$ *(**2**), and* $[Dy^{III}_2Co^{III}_2(OMe)_2(mdea)_2(acac)_4(NO_3)_2]$ *(**3**).* Single-crystal X-ray diffraction measurements revealed that compounds **1** and **3** crystallize in the triclinic space group $P\bar{1}$, whereas compound **2** crystallizes in the monoclinic space group $P2_1/c$. Compounds **1**−**3** (Figures 1 (**2** and **3**) and S1 (**1**)) were all found to be heterometallic tetranuclear clusters consisting of two Co^{III} and two Dy^{III} ions, with the asymmetric unit (ASU) containing half of the complex (one Co^{III} ion and one Dy^{III} ion) which lies upon an inversion center. The metallic core for each cluster displays a planar butterfly motif with the two Dy^{III} ions occupying the body positions and the Co^{III} ions occupying the outer wing-tip sites. These core ions are held together primarily via two μ_3 methoxide (**1** and **3**) or μ_3 hydroxide (**2**) ligands. Around the periphery of each cluster are two amine-based diol or triol ligands that coordinate via the N atom to the Co^{III} ions and then bridge the Co^{III} to the Dy^{III} ions via two μ_2 O atoms. In the cases of **1** and **2**, the third protonated alcohol arm of the $teaH^{2-}$ ligands are noncoordinating. It was then found that one acac ligand chelates to each Co^{III} ion, with one acac and one nitrate both found to chelate to the Dy^{III} ions, thus completing the coordination sphere for each ion. This results in the Co^{III} ions being six-coordinate with an octahedral geometry that displays an average Co−$L_{N,O}$ bond distance of 1.91 Å. The Dy^{III} ions are all eight-coordinate with a distorted square antiprismatic geometry and average Dy−O bond lengths of 2.38, 2.38, and 2.37 Å for **1**−**3**, respectively. Overall, these complexes are identical from a first-coordination environment point of view, with selected bond lengths and angles for **1**−**3** being given in Table 2, which follows the labeling scheme that was used in Figure 2. The structural differences within each cluster are observed only via the alkyl chain size and the OH substituent associated with the third nonbonding arm of the $teaH^{2-}$ ligands, as well as the bridging μ_3 methoxide/hydroxide ligand. Intermolecular packing interactions result in 1-D hydrogen-bonded chains for **1**, with {O−H···O} hydrogen bonds observed between the free protonated alcohol arm of the $teaH^{2-}$ ligand and a neighboring nitrate ion (Figure S2). As a consequence of the $P2_1/c$ space group for **2**, the orientation of the neighboring molecules differs, which results in a 2-D hydrogen-bonded sheet. The hydrogen bonds are now formed between the hydroxide ligand and the noncoordinating arm of the protonated $teaH^{2-}$ ligand of a neighboring cluster, which in turn hydrogen bonds to an O atom of a acac ligand (Figure S3). Compound **3** displays no intermolecular hydrogen bonds because of the absence of the free −OH arm derived from the $teaH^{2-}$ ligand seen in **1** and **2**. It is found, however, that the packing arrangement is similar to that of **1** (Figure S4).

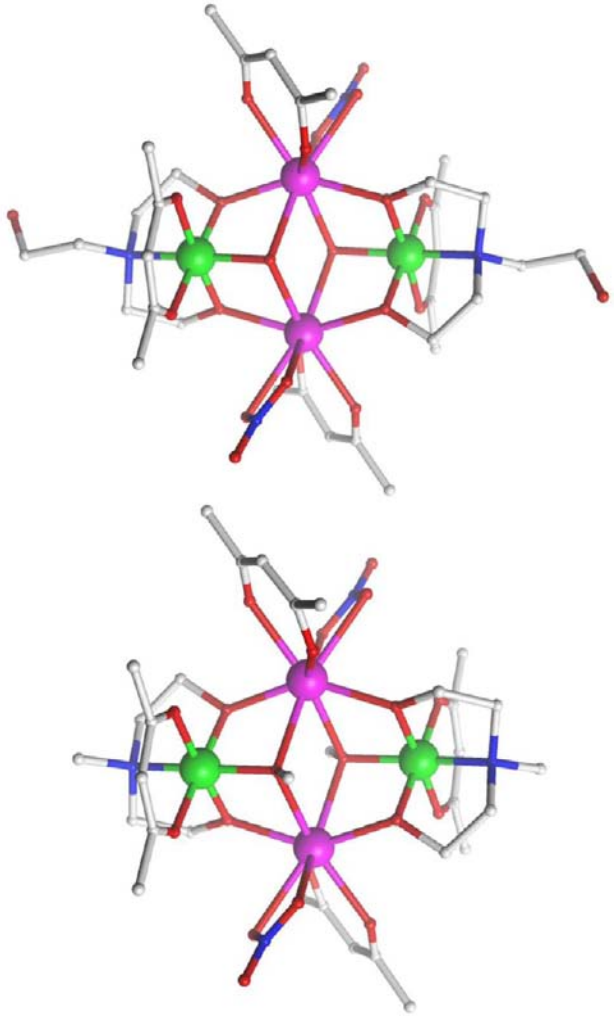

Figure 1. Molecular structures of **2** (top) and **3** (bottom) that highlight the μ_3-OH (**2**) and μ_3-OMe (**3**) bridging ligands and the differing ligand backbones associated with the amine-based polyalcohol ligands. The hydrogen atoms are omitted for clarity. Color scheme: Co^{III}, green; Dy^{III}, purple; O, red; N, blue; C, light gray.

As alluded to earlier, this type of complex with this particular metallic-core motif has recently been reported by our group as part of a structural and magnetic study utilizing carboxylate and amine-based diol or triol ligands with cobalt and lanthanide

dx.doi.org/10.1021/ic400789k | Inorg. Chem. 2013, 52, 7183−7192

Table 2. Selected Bond Distances (Angstroms) and Angles (Degrees) for Complexes 1−3

	1	2	3
Dy1−O3′	2.248(4)[a]	2.255(4)[b]	2.240(4)[c]
Dy1−O2	2.261(4)	2.300(4)	2.270(5)
Dy1−O8	2.277(5)	2.328(4)	2.262(4)
Dy1−O7	2.328(4)	2.243(4)	2.317(5)
Dy1−O1	2.416(5)	2.365(3)	2.411(4)
Dy1−O10	2.459(5)	2.422(4)	2.423(5)
Dy1−O1′	2.512(4)[a]	2.449(4)[b]	2.510(4)[c]
Dy1−O9	2.540(5)	2.554(4)	2.549(4)
Co1−O3	1.871(4)	1.874(4)	1.869(4)
Co1−O2	1.886(4)	1.897(4)	1.883(3)
Co1−O6	1.893(4)	1.891(4)	1.896(4)
Co1−O5	1.903(4)	1.903(4)	1.906(4)
Co1−O1	1.949(4)	1.943(4)	1.936(4)
Co1−N1	1.984(5)	1.975(4)	1.962(5)
Dy1···Dy1′	4.077(5)	3.925(6)	4.052(4)
Dy1···Co1	3.284(5)	3.260(4)	3.297(4)
Dy1′···Co1	3.379(4)	3.362(4)	3.384(2)
Dy1−O1−Dy1′	111.63(4)	109.23(4)	110.83(4)

[a]Symmetry transformation: 1 − *x*, −*y*, 1 − *z*. [b]Symmetry transformation: 2 − *x*, 2 − *y*, −*z*. [c]Symmetry transformation: −*x*, −*y*, 1 − *z*.

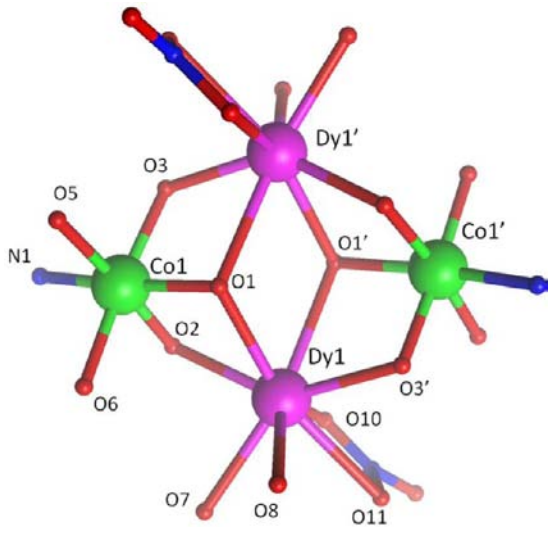

Figure 2. Labeled core structure for compounds **1**−**3**.

ions.[12] Several subtle variations within this system (e.g., the replacement of various $RN(CH_2CH_2OH)_2$ (R = H, Me, Bu) ligands with triethanolamine) resulted in changes to the coordination sphere around the Dy^{III} ion, which gave unique single-molecule magnet behavior for each complex. A comparison of the complex $[Dy^{III}_2Co^{III}_2(OMe)_2(dea)_2(O_2CPh)_4(MeOH)_4](NO_3)_2$ (dea^{2-} = doubly deprotonated diethanolamine)[12b] to compound **1** is shown in Figure 3.

It was found that the central bridging motif between the paramagnetic Dy^{III} ions (i.e., two μ_3 alkoxide or hydroxide ligands) as well as the coordination of the alcohol ligands bridging the Co^{III} to the Dy^{III} ions remains the same. The major difference is that the four benzoate ligands have been replaced by four acac ligands that each chelate to one ion, as opposed to the benzoate ligands that are bridging. As a consequence of this, two nitrate ions are also coordinated to the Dy^{III} site, resulting in two chelating groups associated with the Dy^{III} ion, differing from that of the previous study (Figure 3, left).[12] The analysis of the coordination geometry of the unique Dy^{III} ion in **1**−**3** with the SHAPE program shows that the dysprosium ion in all three compounds resides in an environment that is closest to a square antiprismatic geometry with continuous shape measures (CShMs) of 1.69, 1.82 and 1.71, respectively.[17] These CShMs are rather large and thus imply that even though the geometry is closest to a square antiprism, it is rather distorted. The next closest coordination geometry is the trigonal dodecahedron, with CShMs of 2.91, 2.38, and 2.79 for **1**−**3**. Hence, the coordination environments around the Dy^{III} ions here are more distorted than that of the previously reported $\{Co^{III}_2Dy^{III}_2\}$-$teaH_3$/benzoate complex, which gave CShMs values of 0.865 and 0.923 for the square antiprismatic geometry of Dy1 and Dy2, respectively (two unique tetranuclear molecules were found in the ASU). This will have an influence on the low-lying electronic structure within each Dy ion, which is responsible for the single-ion magnetic properties and hence will likely lead to differing dynamic magnetic behaviors.[11]

Magnetic Measurements. *dc Magnetic Susceptibility Measurements.* The bulk magnetic properties of **1**−**3** were probed via variable-temperature measurements on polycrystalline samples in applied dc fields of 0.1 and 1 *T*. These experiments are plotted as $\chi_M T$ versus *T* (Figure 4) and reveal room-temperature $\chi_M T$ values of 27.75, 27.98, and 27.83 cm^3 mol^{-1} K, for **1**−**3**, respectively, which are in good agreement with the expected value of 28.34 cm^3 mol^{-1} K for two uncoupled Dy^{III} ions ($^6H_{15/2}$, $S = {}^5/_2$, $L = 5$, $J = {}^{15}/_2$, $g_J = {}^4/_3$, and $C = 14.17$ cm^3 mol^{-1} K). As the temperature is lowered,

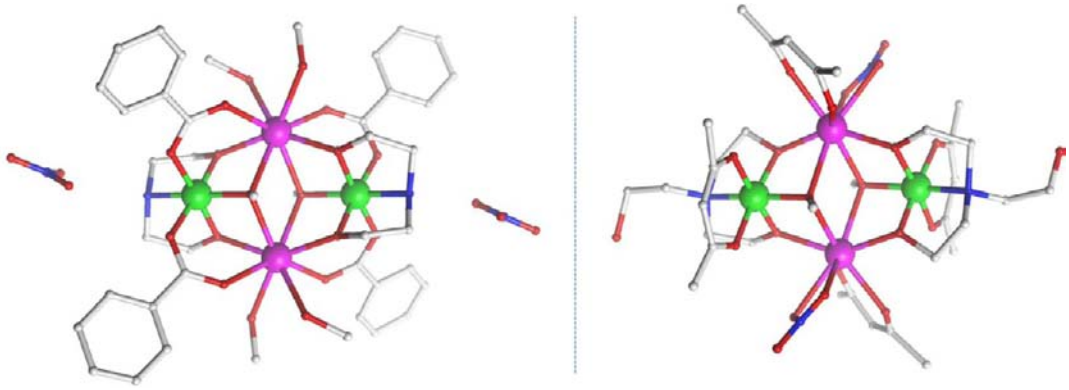

Figure 3. Comparison of $[Dy^{III}_2Co^{III}_2(OMe)_2(dea)_2(O_2CPh)_4(MeOH)_4](NO_3)_2$ (left) to complex **1** (right).

dx.doi.org/10.1021/ic400789k | *Inorg. Chem.* 2013, 52, 7183−7192

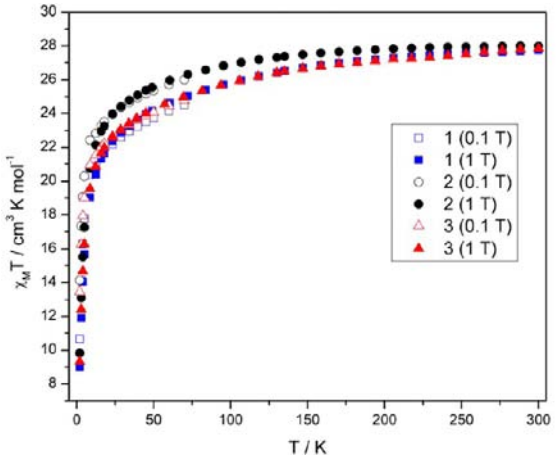

Figure 4. Plots of $\chi_M T$ vs T for **1**−**3** measured in dc fields of 0.1 (2−70 K) and 1 T (2−300 K).

the χ_MT values decrease very gradually (300−50 K) before a more pronounced decrease occurs below 50 K, reaching values of 10.65, 14.12, and 13.46 cm^3 mol^{-1} K at 0.1 T and 2 K for **1**, **2**, and **3**, respectively. The decrease in $\chi_M T$ in all cases is attributed to the depopulation of the m_J sublevels of the ground J multiplet, with the possibility of weak antiferromagnetic exchange and dipolar interactions also contributing to the behavior. The magnetization studies are plotted as M versus H, shown in Figures S5−S7, and each shows a sharp increase with increasing H at low fields and temperatures, with M then increasing linearly at larger fields, reaching values of 9.74, 10.38, and 10.06 Nβ at 2 K and 5 T for **1**, **2**, and **3**, respectively. These are lower than the expected saturation value for two Dy^{III} ions as a result of crystal-field effects eliminating the 16-fold degeneracy of the $^6H_{15/2}$ ground state.

ac Magnetic Susceptibility Measurements. The temperature and frequency dependence of the ac susceptibility under a 3.5 Oe oscillating ac field and zero applied dc magnetic field was determined for compounds **1**−**3**, with SMM behavior observed in all cases. Compounds **1** and **2**, which differ only by the presence of a μ_3 bridging methoxide in **1** and a hydroxide ion in **2**, display very similar dynamic magnetic behavior. The frequency and temperature dependence of the out-of-phase (χ_M'') susceptibility is shown in Figure 5 for **1** and Figure S8 for **2**. The temperature-dependent data for **1** and **2** reveal a significant out-of-phase signal below 18 K, with a broad increase at higher frequencies that reaches a plateau at ∼10 K before increasing again at lower temperatures. This observation suggests that a thermally activated relaxation mechanism is present that crosses over to a temperature-independent regime at lower temperatures, as is often observed for lanthanide-containing systems.[13] A frequency-dependent susceptibility plot confirmed this behavior, with peak maxima observed in χ_M'' with frequencies that became temperature-independent below 5 K, indicating a pure quantum regime. The tunneling frequency was found to be 272 Hz for both complexes, which corresponded to a tunneling time (τ_{QTM}) of 0.58 ms and is of a similar scale to those of other previously reported lanthanide SMMs.[5i] Above 5 K, the relaxation times become temperature-dependent and eventually display Arrhenius behavior associated with a thermally activated mechanism. At temperatures greater than 7.5 K, plots of ln(τ) versus 1/T are linear and fit the Arrhenius law [$\tau = \tau_o \exp(U_{eff}/k_B T)$], affording values of U_{eff} = 27 K and $\tau_o = 8.1 \times 10^{-6}$ s (R = 0.975) for **1** and U_{eff} = 28 K and $\tau_o = 7.4 \times 10^{-6}$ s (R = 0.965) for **2** (Figure 6). Cole−Cole plots of **1** (Figure S9) were constructed and fitted to a generalized Debye model to determine the α values and relaxation times (τ) in the range of 9.5−1.9 K. At high temperatures, the α value is 0.17, which increases to 0.27 upon lowering the temperature to 1.9 K, indicating that a fairly narrow distribution of relaxation times occurs within this temperature range. Interestingly, above 9.5 K

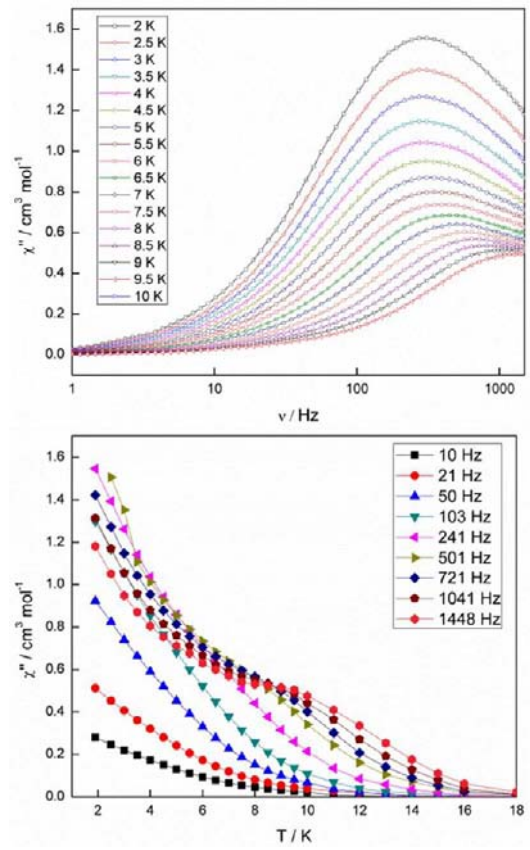

Figure 5. Frequency (top) and temperature (bottom) dependence of the out-of-phase ac susceptibility (χ_M'') of **1** in a zero applied dc magnetic field. The solid lines join the data points.

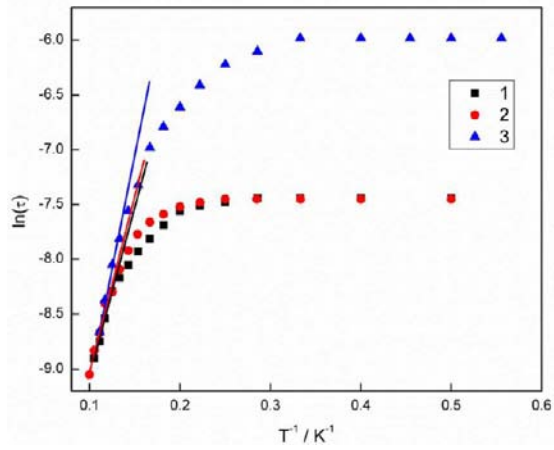

Figure 6. Magnetization relaxation time (τ) plotted as ln(τ) vs T^{-1} for compounds **1**−**3**. The solid lines represent fits to the Arrhenius law of the thermally activated relaxation.

dx.doi.org/10.1021/ic400789k | Inorg. Chem. 2013, 52, 7183−7192

a second increase starts to appear in χ_M'', possibly indicating the presence of a second, faster relaxation mechanism (Figure S10, top left). Because this second increase occurs at frequencies greater than 1500 Hz, which is the limit of our SQUID magnetometer, we were unable to investigate this further.

Compound **3** displays similar but subtly different dynamic magnetic behavior. The temperature dependence of the out-of-phase susceptibility (Figure 7, bottom) again displays

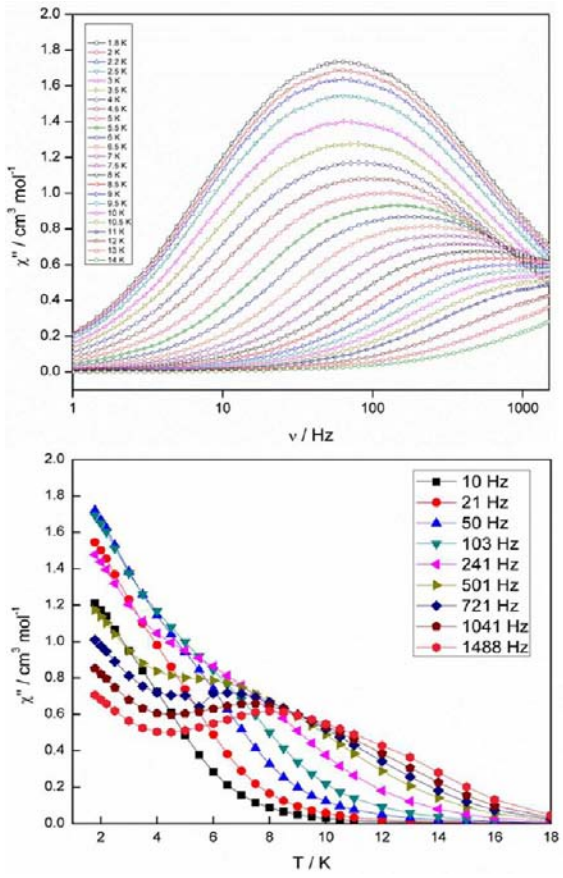

Figure 7. Frequency (top) and temperature (bottom) dependence of the out-of-phase ac susceptibility (χ_M'') of **3** in a zero dc magnetic field. The solid lines join the data points.

frequency-dependent signals below 18 K. At the higher frequencies, a very broad increase is observed, reaching a maximum at ~8 K, which is followed by a second increase at very low temperatures. This broad signal at high frequencies may possibly be due to the second relaxation pathway that was hinted at for compound **1**. The appearance of the peak maxima in the thermally activated region may suggest that the quantum tunneling relaxation pathway occurs at a slower rate in **3** than in **1** and **2**. This was confirmed by the frequency-dependent data (Figure 7, top) in which we now observe a temperature-independent regime below 3 K with a characteristic tunneling frequency of 63 Hz, corresponding to a slower tunneling time of 2.52 ms. Again, a thermally activated mechanism is in operation above 7 K, and the plots of $\ln(\tau)$ versus $1/T$ are linear (Figure 6). Fitting the data to the Arrhenius law $[\tau = \tau_o \exp(U_{eff}/k_BT)]$ afforded values of U_{eff} = 38 K and $\tau_o = 2.6 \times 10^{-6}$ s (R = 0.981) (Figure 6). Cole−Cole plots of **3** (Figure S11) were again constructed and fit to a generalized Debye model to determine the α values and relaxation times (τ) in the range of 15−1.8 K. The α value is 0.15 at 15 K and increases to 0.37 at 1.8 K, showing a substantial broadening of the distribution of relaxation times as the temperature is lowered. Again, above 9 K a second increase in χ_M'' is clearly apparent in this sample, confirming the presence of a second, faster relaxation mechanism that is similar to that of **1** (Figure S10, top right). The second increase again occurs at frequencies greater than 1500 Hz, which is the limit of our SQUID magnetometer, and unfortunately we are unable to investigate this aspect further. Because of the slow magnetic relaxation observed via the ac data for **1**−**3**, hysteresis in M versus H was investigated at 1.8 K but was not detected, probably because of fast quantum tunneling.

Upon comparison of compounds **1**−**3** to the previously reported $\{Co^{III}_2Dy^{III}_2\}$ butterfly clusters,[12] the data revealed a marked difference in the dynamic magnetic behavior in zero dc field. In the previously reported complexes, large thermal energy barriers were reported with values of between 79 and 115 K and with relatively slow QTM. Compounds **1**−**3**, however, display a much smaller anisotropy barrier, faster QTM, and a second relaxation mechanism that is observable in the Cole−Cole plots, a behavior that is intriguing given the single, crystallographically unique Dy^{III} ion present in this case. Future theoretical calculations could potentially determine why there is such a difference in the anisotropy barriers and will possibly shed some light on the observation of multiple relaxation mechanisms.

In systems that display significantly fast quantum tunneling rates, the application of a static dc field will shift $\chi_M''_{max}$ to lower frequencies until the optimal field in which the QTM is efficiently reduced is reached, after which point further increases will lead to a gradual frequency increase in $\chi_M''_{max}$. These experiments may also help to determine if multiple relaxation processes are active by shifting the relaxation mechanism(s) to the time scale of the experiment. The ac susceptibility data were therefore investigated as a function of the applied static field, and experiments were performed at 2 K with a dc field that varied between 0 and 10 000 Oe, revealing unusual and unexpected behavior (Figure 8). For compound **1**, there is an appearance of a second peak in χ_M'' as the field is increased, which is found at very low frequencies whose intensity increases at the expense of the high-frequency peak. This indicates that two mechanisms of relaxation are clearly active with time scales that differ by orders of magnitude. Pathway A is denoted as the fast (high-frequency) process, whereas pathway B is denoted as the slow (low-frequency) process. Pathway A displays a shift in $\chi_M''_{max}$ to lower frequencies (i.e., a longer relaxation time) in fields of up to 1000 Oe before an up-frequency shift is observed, which speeds up the relaxation time between 1000 and 1750 Oe and is followed by a second down-frequency shift. The optimal field was found to be at ~3000 Oe at a frequency of 28 Hz (Figure 8, top right). The increase in relaxation time between 1000 and 1750 Oe is likely due to quantum tunneling mechanisms that become active as a result of level crossings coming into resonance. Increasing the magnetic field past the most efficient field results in a gradual upshift in frequency, yielding faster relaxation rates, which are a feature that is usually observed in SMMs. At fields between 3250 and 5500 Oe (Figure 8, bottom left), it is clear that the out-of-phase susceptibility peaks of pathway A diminish with the appearance of a second, lower-frequency process (pathway B). The two peaks are clearly

dx.doi.org/10.1021/ic400789k | Inorg. Chem. 2013, 52, 7183−7192

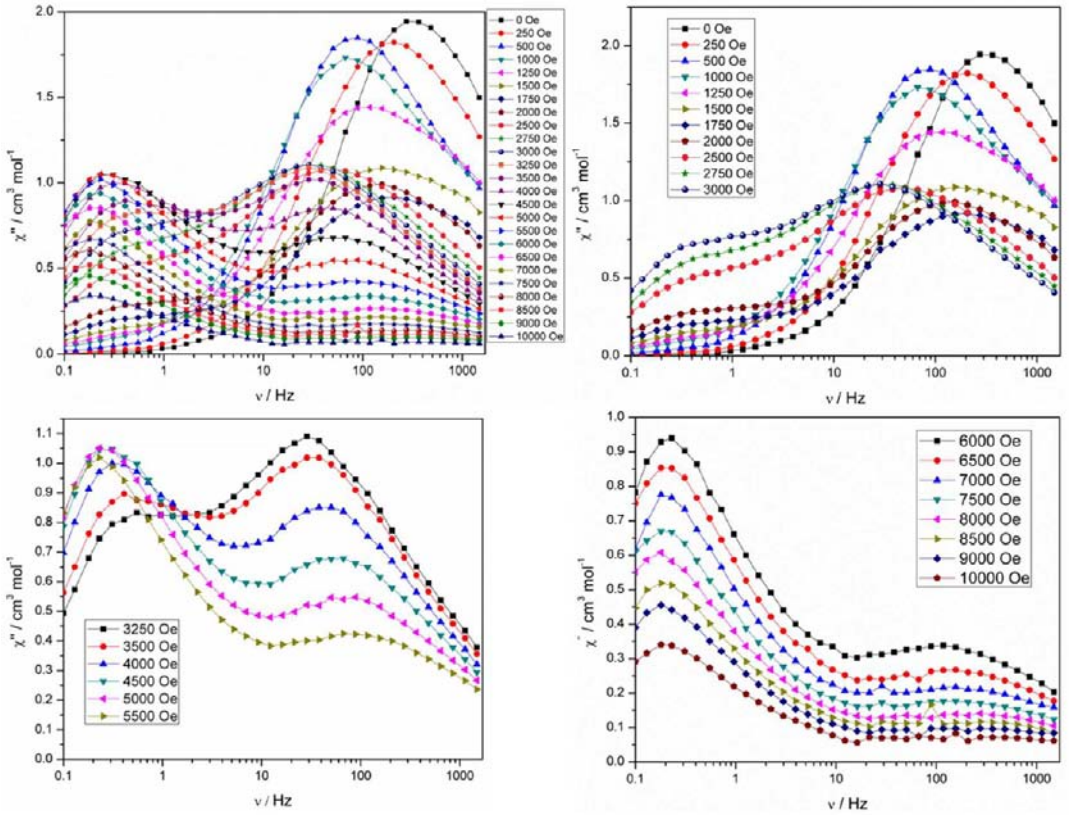

Figure 8. Plots of χ_M'' vs frequency at 2 K for **1** under the application of variable dc fields ranging from 0 to 10 000 Oe. The frequency dependence over the entire field range (top left). The frequency dependence at low fields between 0 and 3000 Oe (top right). The frequency dependence at mid-range fields between 3250 and 5500 Oe (bottom left). The frequency dependence at high fields between 6000 and 10 000 Oe (bottom right). The solid lines join the data points.

observable in this field range. After the appearance of pathway B at higher fields, we see a shift to lower frequencies upon increasing the field, with optimum fields found above 6000 Oe at a frequency of 0.23 Hz. Figure 8 (bottom right) shows the appearance of pathway B at the expense of pathway A at the highest fields measured (> 6000 Oe).

Thus, variable temperature and frequency measurements for **1** at the optimal field of 3000 Oe for pathway A were recorded. A second measurement at a field of 6000 Oe was also performed to highlight the appearance of pathway B and to study its temperature dependence. These plots are shown in Figure 9. The relaxation times were extracted from the high-frequency data at 3000 Oe (Figure 9, top), and it was found that the relaxation follows a thermally activated mechanism above 7.5 K with plots of $\ln(\tau)$ versus $1/T$ that are linear (Figure S12). Fitting the data to the Arrhenius law $[\tau = \tau_o \exp(U_{eff}/k_BT)]$ afforded values of U_{eff} = 35 K and $\tau_o = 3.37 \times 10^{-6}$ s (R = 0.991) (pathway A). The anisotropy barrier increases to a small extent, and as expected no crossover into a pure quantum regime above 1.9 K was observed as a result of the application of the static field that reduces the QTM. The appearance of the second, slower process also became evident. Cole−Cole plots of **1** at 3000 Oe (Figures 10, top and S13) were constructed and fit to a generalized Debye model to determine the α values and relaxation times (τ) in the range of 10−1.9 K. At low temperatures (1.8−6 K), two overlapping semicircles are clearly present, indicating two mechanisms of relaxation at differing time scales (Figure 10, top). Above 6 K, the slow process disappears (Figure S13); however, above 9 K, a second increase again appears in χ_M'' that is identical to the zero field measurements (Figure S10, bottom), indicating the presence of three separate relaxation mechanisms in this system (pathway C). At 1.9 K, the fast relaxation process (A) has a characteristic time of 0.219 s and an α value of 0.47, whereas the slow process (B) has a characteristic time of 17.5 s and an α value approaching zero, indicating that the slow process has a very narrow distribution of relaxation times and the fast process is substantially broader in its distribution. As the temperature is increased to 3 K, the fast process undergoes a reduction in the characteristic time, as expected, to 83.9 ms and a slight reduction in the α value to 0.45, whereas the slow process also speeds up, showing a characteristic time of 12.9 s with an α-value that remains essentially zero. Above this temperature, the slower process begins to disappear and the generalized Debye data for these temperatures are not reliable; however, we are still able to fit the data to a two-barrier relaxation model to avoid skewing the results for the faster process. At 6 K, the fast process has a characteristic time of 18.6 ms and an α value of 0.28, indicating that the distribution of relaxation times becomes much more narrow at higher temperatures. Above 6 K, the slower process is not observable, and the fit of the data to the generalized Debye model using one or two processes gave the same result. At 10 K, the fast process shows a characteristic time of 4.30 ms with an α value of 0.11, showing an extremely narrow distribution of relaxation times at these higher temperatures.

The 6000 Oe plot highlights both relaxation pathways that are observable (A + B). The fast process follows a similar

dx.doi.org/10.1021/ic400789k | Inorg. Chem. 2013, 52, 7183−7192

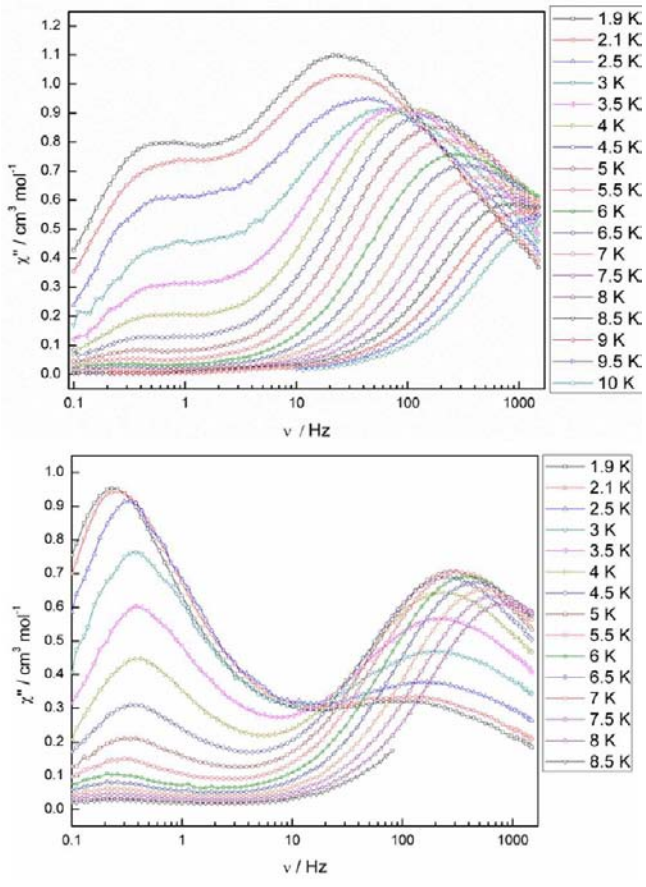

Figure 9. Frequency dependence of the out-of-phase ac susceptibility (χ_M'') of **1** in a 3000 (top) and 6000 Oe (bottom) applied dc magnetic fields. The solid lines join the data points.

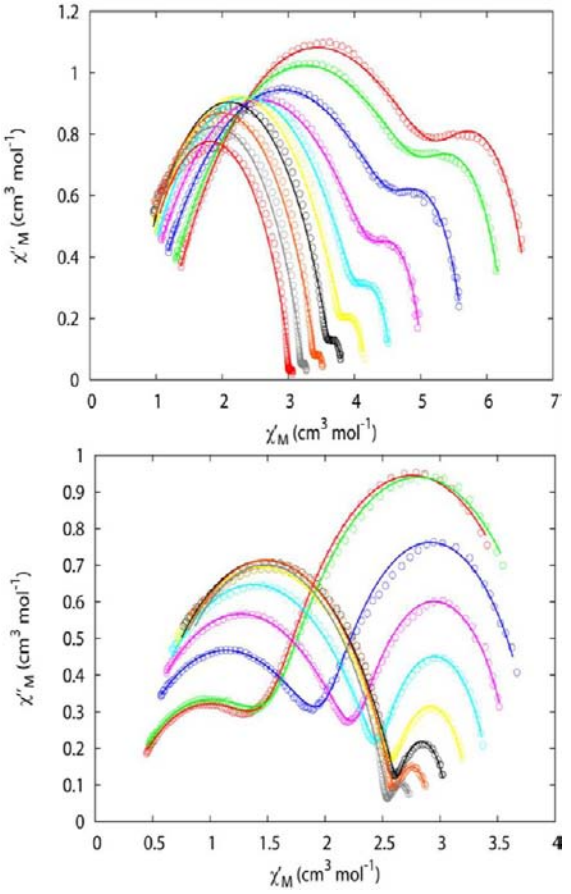

Figure 10. Cole−Cole plots of **1** at applied fields of 3000 (top) and 6000 Oe (bottom) and at temperatures between 1.9 (red) and 6 K (gray) for both. The solid lines are the fits of the experimental data using a generalized Debye model.

temperature dependence to the 0 and 3000 Oe measurements; however, the slow relaxation pathway (low frequency) exhibits behavior that is intriguing. At 1.9 K, the peak maxima in χ_M'' is found at 0.23 Hz and increasing the temperature shifts this to 0.38 Hz at 3 K, as expected. As the temperature is increased further, the relaxation time slows down unusually with maxima found at 0.21 Hz above 6 K. It is therefore seen that the time scale of the relaxation mechanism is close to being temperature-independent with the χ_M'' value also diminishing significantly upon increasing the temperature. It seems apparent that population effects are important, as the percentage susceptibility of the fast process increases at the expense of the slow process as the temperature increases, which is almost the opposite effect that the applied dc field produced on the sample. This is a possible indication that the separate relaxation processes may occur via first excited (slow) and second excited (fast) states. Cole−Cole plots at 6000 Oe again show that two semicircles are clearly observable up to 6 K (Figure 10, bottom), above which temperature the second process disappears (Figure S14). At 1.9 K, the slow process has a characteristic time of 27.0 s and an α value of 0.17, whereas the fast process has a characteristic time of 55.9 ms and an α value of 0.50, indicating that it has an extremely broad distribution of relaxation times compared to the slow process. Increasing the temperature to 6 K narrows the distributions of both processes, with the slow process having a characteristic time of 26.5 s and an α value of zero, whereas the fast process has a characteristic time of 14.8 ms and an α value of 0.27. At 8 K, the slow process has entirely disappeared and the fast process now has a characteristic time of 8.54 ms and an α value of 0.31, which show that it has unusually slightly broadened.

It has previously been noted for polynuclear lanthanide complexes possessing distinct anisotropy centers (i.e., more than one unique coordination environment) that multiple relaxation modes can be observed for differing time scales, as the single ion behavior often dominates the molecular behavior.[10] In the present case, however, the molecule displays one unique Dy^{III} coordination environment because the second ion is crystallographically equivalent to it. The appearance of a second relaxation pathway upon the application of a static dc field has been observed in a small number of monomeric and dimeric cases containing equivalent Dy^{III} sites, similar to the situation that we observed for **1**, including the $[Dy(DOTA)]$,[18] $[Cp_2Dy(thf)(\mu\text{-}Cl)]_2$,[19] $[Dy(COT'')_2Li(THF)(DME)]$,[20] and $[Co(SPh)_4]^{2-}$ complexes.[21] These compounds display a second, slower process in applied fields, displaying a temperature-dependent thermally activated relaxation mechanism. This is the opposite of what was observed in the case of **1**, and further investigations are warranted to try and shed some light on these new observations.

Compound **3** also displays similar field-dependent behavior to that of **1** at 2 K, as shown in Figure S15. Two relaxation modes are observed upon the application of a static dc field, with the appearance of the second slow mechanism appearing at the expense of the faster mechanism. It is observed that the

dx.doi.org/10.1021/ic400789k | Inorg. Chem. 2013, 52, 7183−7192

optimal fields are found at 500 and 2750 Oe for the fast process, with the appearance of the second slower process becoming observable between 3000 and 4000 Oe. Again, at higher fields the slow process is dominant and the disappearance of the high-frequency peaks occurs.

Although the dynamic magnetic behavior for **1** and **2** is similar to that of **3**, it is apparent that there are obvious differences, even though their first-coordination sphere is identical. The relaxation barriers that were determined from the ac data differ in zero field, with pure quantum regimes occurring at differing tunneling frequencies. These systems are therefore ideal for further study to better understand the single-molecule behavior of dinuclear lanthanide complexes.

Recent studies of dinuclear dysprosium complexes diluted with an isostructural Y^{III} diamagnetic matrix have shown that the slow relaxation mechanism of the whole complex in such weakly coupled systems is of single-ion origin and have displayed the importance of the neighboring ion upon the zero field quantum tunneling time scale.[12a,22] The preparation of a 5% Dy-doped sample resulted in a complex containing three possible products (ignoring the Co^{III} ions), namely, the $\{Y^{III}_2\}$, $\{Y^{III}Dy^{III}\}$, and $\{Dy^{III}_2\}$ species. The probability of observing the different dinuclear species at the 5% dysprosium dilution level is 90.25% for $\{Y^{III}_2\}$, 9.5% for $\{Y^{III}Dy^{III}\}$, and 0.25% for $\{Dy^{III}_2\}$. Therefore, the major paramagnetic product will be the single ion $\{Y^{III}Dy^{III}\}$ species. ac measurements were performed in a zero applied dc field on a 5:95 Dy/Y sample of **1**. The data show a similar slow magnetic relaxation below 18 K to $\{Dy^{III}_2\}$ complex **1**, with frequency-dependent out-of-phase signals indicating that the slow relaxation is of single-ion origin (Figure 11). It appears that the plateaus observed in the $\{Dy^{III}_2\}$ species

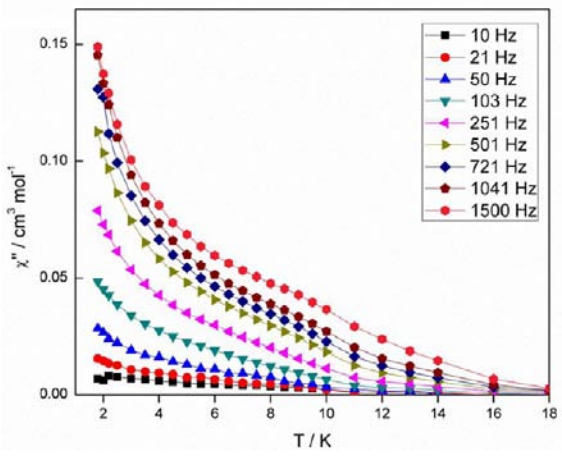

Figure 11. Temperature dependence of the out-of-phase susceptibility (χ_M'') for the 5:95 Dy/Y sample of **1**. The solid lines join the data points.

are now obscured by a second, more prevalent increase at lower temperatures, indicating that quantum tunneling is very efficient at zero field in this dilute sample. This can also be observed via the frequency-dependent plot shown in Figure S16. It therefore shows the importance that the neighboring ions play in modulating the dynamic magnetic behavior in single-ion-based molecular magnets.

Field-dependent ac measurements were again performed on the dilute sample, with the isofield χ_M'' versus frequency plots being shown in Figure S17. Again, at low fields (<1000 Oe) we observe peak maxima in χ_M'' at high frequencies that shift to lower frequencies upon the application of larger fields. Above 1250 Oe, we observe a broadening of these peaks until a new second peak becomes observable at the expense of the first peak, with a further increase becoming apparent at even lower frequencies, indicating a third process. At the highest fields measured (>4500 Oe), only the low-frequency increase is observable with the maxima lying below the minimum frequency of our instrument. This again shows that there are multiple mechanisms that are of single-ion origin. These data may confirm that there are greater than two relaxation mechanisms active in compound **1**, but again it appears that the dynamics are greatly affected by the neighboring ion because maxima appear at differing frequencies between the pure and dilute samples.

CONCLUSIONS

Three new heterometallic tetranuclear $\{Co^{III}_2Dy^{III}_2\}$ complexes have been isolated utilizing triethanolamine or methyldiethanolamine and acetyacetonate as bridging ligands. All complexes display a butterfly metallic-core arrangement and are similar to our previously reported heterometallic SMMs.[11] ac magnetic susceptibility measurements confirm that single molecule magnet behavior is displayed in zero dc magnetic field with thermally activated anisotropy barriers of 27, 28, and 38 K. It is also observed that a second, faster relaxation process may be present at frequencies greater than 1500 Hz. We have also shown via dilution studies of the Dy^{III} sample within a Y^{III} diamagnetic matrix that the single-molecule magnet behavior is single ion in origin. The dynamic magnetic behavior observed for compounds **1**−**3** is similar overall, but it does display some subtle differences such as the barrier height and the occurrence of a pure quantum regime at differing time scales (between **1** and **3**). The present complexes differ significantly from previously reported $\{Co^{III}_2Dy^{III}_2\}$ SMM complexes.[12] SHAPE calculations have revealed significant distortions of the local Dy^{III} ion geometry in the present complexes in comparison to those in the previous complexes, which likely accounts for the differences between them. Upon the application of a static dc field to **1** and **3**, further relaxation mechanisms are observed for each sample as shown via the appearance of a slower, temperature-independent relaxation mechanism that occurs at the expense of the more prominent faster relaxation mode. The appearance of multiple relaxation mechanisms in the present complexes may be due to the significantly distorted square antiprismatic geometry of **1**−**3** that lowers the local symmetry of the ion. There is much that is yet to be rationalized regarding these relaxation effects, and further investigations are underway using related complexes that we have recently synthesized. These studies will be reported in due course.

ASSOCIATED CONTENT

Supporting Information

Crystallographic data in CIF format, molecular structure of **1** and packing diagrams of **1**−**3**, dc magnetic data, ac magnetic data for compounds **1**−**3**, and ac plots of the 5% Dy^{III}-doped sample in a diamagnetic Y^{III} matrix. This material is available free of charge via the Internet at http://pubs.acs.org.

AUTHOR INFORMATION

Corresponding Author

*E-mail: keith.murray@monash.edu.

Notes

The authors declare no competing financial interest.

■ ACKNOWLEDGMENTS

K.S.M. thanks the Australian Research Council (ARC) and the Australia-India Strategic Research Fund (AISRF) for their support of this work. The Australian Synchrotron is also thanked for their help and access to the MX1 beamline.

■ REFERENCES

(1) (a) Zhang, P.; Guo, Y-N; Tang, J. *Coord. Chem. Rev.* **2013**, *257*, 1728. (b) Habib, F.; Murugesu, M. *Chem. Soc. Rev.* **2013**, *42*, 3278. (c) Sessoli, R.; Powell, A. *Coord. Chem. Rev.* **2009**, *253*, 2328. (d) Clemente-Juan, J. M; Coronado, E.; Gaita-Arino, A. *Chem. Soc. Rev.* **2012**, *41*, 7464.

(2) Christou, G.; Gatteschi, D.; Hendrikson, D. N.; Sessoli, R. *MRS Bull.* **2000**, *25*, 66.

(3) (a) Leuenberger, M.; Loss, D. *Nature* **2001**, *410*, 789. (b) Aromi, G.; Aguila, D.; Gamez, F.; Luis, F.; Roubeauc, O. *Chem. Soc. Rev.* **2012**, *41*, 537. Bogani, L.; Wernsdorfer, W. *Nat. Mater.* **2008**, *7*, 179. (c) Ardavan, A.; Rival, O.; Morton, J. J. L.; Blundell, S.; Tyryshkin; Timco, G.; Winpenny, R. E. P. *Phys. Rev. Lett.* **2007**, *98*, 057201. (d) Vincent, R.; Klyatskaya, S.; Ruben, M.; Wernsdorfer, W.; Balestro. *Nature* **2012**, *488*, 357. (e) Van Der Zant, H. S. J. *Nat. Nanotechnol.* **2012**, *7*, 555. (f) Wernsdorfer, W. *Nat. Nanotechnol.* **2009**, *4*, 145. (g) Urdampilleta, M.; Klyatskaya, S.; Cleuziou; Ruben, M.; Wernsdorfer, W. *Nat. Mater.* **2011**, *10*, 502.

(4) Ishikawa, N.; Sugita, M.; Ishikawa, T.; Koshihara, S.; Kaizu, Y. *J. Am. Chem. Soc.* **2003**, *125*, 8694.

(5) (a) Chilton, N. F.; Langley, S. K.; Moubaraki, B.; Soncini, A.; Batten, S. R.; Murray, K. S. *Chem. Sci.* **2013**, *4*, 1719. (b) Jiang, S.-D.; Liu, S.-S.; Zhou, L.-N.; Wang, B.-W.; Wang, Z.-M.; Gao, S. *Inorg. Chem.* **2012**, *51*, 3079. (c) Jiang, S.-D.; Wang, B.-W.; Sun, H.-L.; Wang, Z.-M.; Gao, S. *J. Am. Chem. Soc.* **2011**, *133*, 4730. (d) AlDamen, M. A; Clemente-Juan, J. M.; Coronado, E.; Marti-Gastaldo, C.; Gaita-Arino, A. *J. Am. Chem. Soc.* **2008**, *130*, 8874. (e) AlDamen, M. A; Cardona-Serra, S.; Clemente-Juan, J. M.; Coronado, E.; Gaita-Arino, A.; Marti-Gastaldo, C.; Luis, F.; Montero, O. *Inorg. Chem.* **2009**, *48*, 3467. (f) Watanabe, A.; Yamashita, A.; Nakano, M.; Yamamura, T.; Kajiwara, T. *Chem.—Eur. J.* **2011**, *17*, 7428. (g) Lin, P.-H.; Burchell, T. J.; Ungur, L.; Chibotaru, L. F.; Wernsdorfer, W.; Murugesu, M. *Angew. Chem., Int. Ed.* **2009**, *48*, 9489. (h) Tian, H.; Zhao, L.; Guo, Y-N; Guo, Y.; Tang, J.; Liu, Z. *Chem. Commun.* **2012**, *48*, 708. (i) Guo, Y.-N.; Xu, G.-F.; Wernsdorfer, W.; Ungur, L.; Guo, Y.; Tang, J.; Zhang, H.-L.; Chibotaru, L. F.; Powell, A. K. *J. Am. Chem. Soc.* **2011**, *133*, 11948. (j) Tuna, F.; Smith, C.; Bodensteiner, M.; Ungur, L.; Chibotaru, L.; McInnes, E.; Winpenny, R.; Collison, C.; Layfield, R. *Angew. Chem., Int. Ed.* **2012**, *51*, 6976.

(6) (a) Blagg, R. J.; Muryn, C. A.; McInnes, E. J. L.; Tuna, F.; Winpenny, R. E. P. *Angew. Chem., Int. Ed.* **2011**, *50*, 6530. (b) Blagg, R. J; Tuna, F.; McInnes, E. J. L.; Winpenny, R. E. P. *Chem. Commun.* **2011**, *47*, 10587. (c) Hewitt, I. J.; Tang, J.; Madhu, N. T.; Anson, C. E.; Lan, Y.; Luzon, J.; Etienne, M.; Sessoli, S.; Powell, A. K. *Angew. Chem., Int. Ed.* **2010**, *49*, 6352. (d) Usman Anwar, M.; Thompson, L.; Nicole Dawe, L.; Habib, F.; Murugesu, M. *Chem. Commun.* **2012**, *48*, 4576.

(7) (a) Guo, Y.-N.; Xu, G.-F.; Guo, Y.; Tang, J. *Dalton Trans.* **2011**, *40*, 9953. (b) Luis, F.; Martínez-Perez, M. J.; Montero, O.; Coronado, E.; Cardona-Serra, S.; Martí-Gastaldo, C.; Clemente-Juan, J. M.; Sese, J.; Drung, D.; Schurig, T. *Phys. Rev. B* **2010**, *82*, 060403. (c) Giraud, R.; Wernsdorfer, W.; Tkachuk, A. M.; Mailly, D.; Barbara, B. *Phys. Rev. Lett.* **2001**, *87*, 057203. (d) Ishikawa, N.; Sugita, M.; Wernsdorfer, W. *J. Am. Chem. Soc.* **2005**, *127*, 3650. (e) Ishikawa, N.; Sugita, M.; Wernsdorfer, W. *Angew. Chem., Int. Ed.* **2005**, *44*, 2931.

(8) Rhinehart, J. D.; Long, J. R. *Chem. Sci.* **2011**, *2*, 2078.

(9) (a) Tang, J.; Hewitt, I.; Madhu, N.; Chastanet, G.; Wernsdorfer, W.; Anson, C.; Benelli, C.; Sessoli, R.; Powell, A. *Angew. Chem., Int. Ed.* **2006**, *45*, 1729. (b) Chibotaru, L. F.; Ungur, L.; Soncini, A. *Angew. Chem., Int. Ed.* **2008**, *47*, 4126. (c) Luzon, J.; Bernot, K.; Hewitt, I. J.; Anson, C. E.; Powell, A. K.; Sessoli, R. *Phys. Rev. Lett.* **2008**, *100*, 247205. (d) Guo, P.-H.; Liu, J.-L.; Zhang, Z.-M.; Ungur, L.; Chibotaru, L. F.; Leng, J.-D.; Guo, F.-S.; Tong, M.-L. *Inorg. Chem.* **2012**, *51*, 1233.

(10) (a) Lin, P.-H.; Sun, W.-B.; Yu, M.-F.; Li, G.-M.; Yan, Y.-F.; Murugesu, M. *Chem. Commun.* **2011**, *47*, 10993. (b) Venugopal, A.; Tuna, F.; Spaniol, T.; Ungur, L.; Chibotaru, L.; Okuda, J.; Layfield, R. *Chem. Commun.* **2013**, *49*, 901. (c) Lin, S.-Y.; Zhao, L.; Guo, Y.-N.; Zhang, P.; Guo, Y.; Tang, J. *Inorg. Chem.* **2012**, *51*, 10522. (d) Guo, Y.-N.; Xu, G.-F.; Gamez, P.; Zhao, L.; Lin, S.-Y.; Deng, R.; Tang, J.; Zhang, H.-J. *J. Am. Chem. Soc.* **2010**, *132*, 8538.

(11) (a) Baldovi, J. J; Cardona-Serra, S.; Clemente-Juan, J. M; Coronado, E.; Gaita-Arino, A.; Palii, A. *Inorg. Chem.* **2012**, *51*, 12565. (b) Baldovi, J. J; Borras-Almenar, J. M; Clemente-Juan, J. M; Coronado, E.; Gaita-Arino, A. *Dalton Trans.* **2012**, *44*, 13705. (c) Sorace, L.; Benelli, C.; Gatteschi, D. *Chem. Soc. Rev.* **2011**, *40*, 3092.

(12) (a) Langley, S. K.; Chilton, N. F.; Ungur, L.; Moubaraki, B.; Chibotaru, L. F.; Murray, K. S. *Inorg. Chem.* **2012**, *51*, 11873. (b) Langley, S. K.; Chilton, N. F.; Ungur, L.; Moubaraki, B.; Wernsdorfer, W.; Chibotaru L. F.; Murray, K. S. Unpublished work.

(13) (a) Guo, Y-N; Chen, X-H; Xue, S.; Tang, J. *Inorg. Chem.* **2011**, *50*, 9705. (b) Lin, P-H; Burchell, T.; Clerac, R.; Murugesu, M. *Angew. Chem., Int. Ed.* **2008**, *47*, 8848. (c) Xu, G-F; Wang, Q-L; Gamez, P.; Ma, Y.; Clerac, R.; Tang, J.; Yan, S-P; Cheng, P.; Liao, D.-Z. *Chem. Commun.* **2010**, *46*, 1506.

(14) McPhillips, T. M.; McPhillips, S. E.; Chiu, H. J.; Cohen, A. E.; Deacon, A. M.; Ellis, P. J.; Garman, E.; Gonzalez, A.; Sauter, N. K.; Phizackerley, R. P.; Soltis, S. M.; Kuhn, P. *J. Synchrotron Radiat.* **2002**, *9*, 401.

(15) Kabsch, W. *J. Appl. Crystallogr.* **1993**, *26*, 795.

(16) Sheldrick, G. M. *Acta Crystallogr.* **2008**, *A64*, 112.

(17) (a) Alvarez, S.; Alemany, P.; Casanova, D.; Cirera, J.; Llunell, M.; Avnir, D. *Coord. Chem. Rev.* **2005**, *249*, 1693. (b) Cirera, J.; Ruiz, E.; Alvarez, S. *Organometallics* **2005**, *24*, 1556.

(18) Car, P.-E.; Perfetti, M.; Mannini, M.; Favre, A.; Caneschi, A.; Sessoli, R. *Chem. Commun.* **2011**, *47*, 3751.

(19) Sulway, S.; Layfield, R.; Tuna, F.; Wernsdorfer, W.; Winpenny, R. *Chem. Commun.* **2012**, *48*, 1508.

(20) Jeletic, M.; Lin, P.-H.; Le Roy, J.; Korobkov, I.; Gorelsky, S.; Murugesu, M. *J. Am. Chem. Soc.* **2011**, *133*, 19286.

(21) Zadrozny, J.; Long, J. *J. Am. Chem. Soc.* **2011**, *133*, 20732.

(22) Habib, F.; Lin, P.-H.; Long, J.; Korobkov, I.; Wernsdorfer, W.; Murugesu, M. *J. Am. Chem. Soc.* **2011**, *133*, 8830.